ISSN 1840-4855
e-ISSN 2233-0046

Original scientific article
http://dx.doi.org/10.70102/afts.2025.1833.483

EFFECT OF WALL GEOMETRY AND RUBBER INCLUSION ON THE BLAST PERFORMANCE OF STRUCTURAL CONCRETE BARRIERS

Islam Ali Mahmoud[1], Ashraf A. A. Beshr[2], Ahmed E. Sedawy[3*]

[1]Assistant Professor, Civil Engineering Department, Delta Higher Institute for Engineering & Technology, Mansoura, Egypt.e-mail: Islam.ali@dhiet.edu.eg, orcid: https://orcid.org/0009-0005-2011-1570
[2]Professor of Surveying and Photogrammetry, Public Works Department, Faculty of Engineering, Mansoura University, Egypt. e-mail: aaabeshr@mans.edu.eg, orcid: http://orcid.org/0000-0002-4083-2245
[3]Assistant Professor, Civil Engineering Department, Misr Higher Institute for Engineering and Technology, Mansoura, Egypt. e-mail: ahmedalsaadawy@engmet.edu.eg, orcid: https://orcid.org/0009-0002-9080-379X

Received: June 19, 2025; Revised: September 03, 2025; Accepted: September 29, 2025; Published: October 30, 2025

SUMMARY

This study presents an advanced nonlinear numerical analysis using ABAQUS to assess the blast resistance of curved rubber-reinforced concrete (RRC) barrier walls. Four types of concrete, normal concrete (NC), and rubberized concretes with 10%, 30%, and 50% rubber particle volume fractions (RC10, RC30, RC50) were modeled and evaluated under blast loading conditions. The numerical approach was validated using a 3D hydro code model, followed by calibration against established experimental benchmarks. The study also examined the influence of wall curvature on blast performance using three curvature angles: 0°, 23°, and 48°. Results demonstrated a clear improvement in blast mitigation with increased curvature. For NC slabs, the peak pressure was reduced from 60.05 MPa (flat) to 50.05 MPa at 48° curvatures. Similar trends were observed for rubberized concretes, with RC30 showing the highest-pressure reduction of 30% at 48°. The curved configurations facilitated more efficient stress redistribution and reduced penetration depth, although high curvature led to localized stress concentrations at slab edges, suggesting the need for targeted reinforcement. Overall, the 48° curved RRC wall configuration provided the most effective blast resistance, regardless of material composition. These findings highlight the advantages of combining geometry optimization and rubber inclusion to enhance the structural performance of protective concrete barriers against explosive loads.

Key words: *rubber concrete slab, finite element analysis, abaqus, curved barrier, dynamic loading.*

INTRODUCTION

Concrete is still the standout among many others as one of the best construction materials all over the world, whose versatility, cost efficiency, and structural effectiveness are not disputed. However, the growing number of terrorist explosions and their serious consequences forced on the most appropriate products have a need for the development of materials, the task of which is to resist the new extreme

dynamic loads. One of the innovative strategies to increase concrete performance significantly in that case is the addition of waste rubber particles, which results in the next material, known as rubberized concrete (RC). The revolutionary substance uses the rubber that was recycled and turns it into a partial aggregate replacement, resulting in possible benefits such as energy dissipation, deformation capacity, and impact resistance [21], [10].

Many papers reported the study of rubberized concrete's dynamic and mechanical characteristics at different strain rate levels and loading conditions. [1],[2] made experimental tests using cracked straight-through Brazilian disc (CSTBD) specimens subjected to high-strain-rate loading by drop hammer impact and split Hopkinson pressure bar apparatus. According to their results, rubberized concrete has higher strain-rate sensitivity than traditional concrete, and they also suggested that the content of rubber should be no more than 30% by volume at most in order to keep the structure intact [24]. The high sensitivity is attributed to the natural flexibility of the rubber particles, which primarily contributes to the superior energy absorption characteristics under dynamic stress conditions. In support of these findings, [2],[3] performed splitting tensile tests on the fiber-reinforced rubberized concrete (FRRC) and showed that the incorporation of fibers enhances tensile performance under high strain rates, effectively inhibiting crack initiation and propagation. Although (4)reported decreasing compressive strength and elastic modulus by substituting coarse aggregate with shredded rubber, which will decrease the wall system's static load capacity. Their results also suggest the detrimental impact, compared to normal concrete, on far-field blast resistance due to such substitutions [1], [6].

In a separate study, (5) investigated the combined influence of waste tire rubber, linear low-density polyethylene (LLDPE), and silica fume on concrete mixtures. They reported that the physical properties of these waste materials had a major influence on impact resistance, and the highest impact resistance was achieved in mixtures with 15% silica fume and 30% LLDPE rubber. In another study, (6,7) utilized the Karagozian and Case (K&C) concrete model to simulate the blast response of rubberized concrete slabs numerically. Their simulation of rubberized concrete slabs proved that rubberized concrete can outperform with respect to blast resistance regardless of the support conditions [4].

To explain the computational methods further, (8) came up with the method of using the finite element model to predict the energy absorption ability of modified rubberized concrete with various impact scenarios. The result that the model produced was that the increase in the rubber content resulted in the maximum energy dissipation; however, it caused a decrease in the compressive strength. Still, the use of supplementary cementitious materials such as 10% rice husk ash could provide a solution to this problem, as it would only improve ductility and strength retention [3].

[5,9] initiated the discussion on the impact performance of plain and rubberized concrete reinforced with hybrid steel-polypropylene (MS and PP) fibers using low-velocity drop hammer tests (impact velocity of 2.8 m/s). The authors' findings were that the post-crack energy absorption and the tensile bond capability increased exponentially with the hybrid fibers, which were of a variety of metals (MS) and polymer (PP). Specifically, the introduction of only the 1.0% MS fiber had no impact on the compressive strength, highlighting the dominant role of fiber synergy in improving impact behavior. While comparing fiber-reinforced concrete, all fiber-reinforced rubberized concrete (FRRUC) specimens exhibited higher first-crack impact energies and ductility indices than standard fiber-reinforced concrete (FRC) specimens did [9].

The damping characteristics in rubberized recycled aggregate concrete and its components, which were performed by numerical analyses, were further advanced by [10]. Moreover, [11] identified the potential of fiber-reinforced recycled aggregate concrete (FRRC) to become a blast-resistant material on the basis of some experimental evidence they proved, i.e., the high strain rate behavior of the material and the immense stress absorption and redistribution capacity during explosive events [29]. New geometry forms, such as convex or concave shapes made from fla

t barrier walls, were experimentally analyzed by [6],[12]for the purpose of best structural transformation from blast pressures, and the obtained results well demonstrated that curved barriers have remarkably higher energy-absorbing capacities. A second study [13]describing the mechanical response to the blast

of ultra-high-performance concrete (UHPC) barrier walls also confirmed the claimed potential benefits of UHPC structures in terms of blast resistance, fragmentation, and structural dismantlement protection and proved that, soon, the rescue of the dwelling zone and infrastructure might be secured.[9],[14]provided additional experimental validation by comparing the performance of ordinary concrete slabs and those incorporating 20% rubber under impact conditions. Their laboratory findings consistently showed a marked reduction in peak stress levels within the rubberized slabs, further substantiating the effectiveness of rubber inclusion in enhancing impact tolerance [8], [11].

Recent research has focused on improving concrete structures' resistance to impact and blast loads. Rubberized concrete barriers show increased flexibility and energy absorption under impact, potentially reducing injuries in accidents [28)]. Studies on reinforced concrete elements reveal that analytical investigations are limited compared to experimental and simulation approaches (16). Reinforced concrete structures typically exhibit brittle damage, localized spallation, and ductile failure modes when subjected to blast loads [27]. Slurry Infiltrated Fiber Concrete (SIFCON), containing up to 20% fiber content, has emerged as a promising material for enhancing impact and blast resistance in critical structures like energy plants and military buildings [18], [15]. These studies collectively contribute to understanding the behavior of concrete structures under extreme loading conditions and offer insights into potential improvements in structural design and material selection for enhanced safety and resilience [17]. [26] Explore the potential of utilizing this green material to construct roadside barriers capable of enduring car collisions. In comparison to conventional concrete barriers, their research shows that the rubberized concrete barrier not only satisfies safety requirements for roadside barriers but also significantly lessens the impact force on cars [12], [25].

The review of the literature above simplifies the fact that rubberized concrete, particularly with the use of fibers and curvature, is highly likely to be a major milestone in the construction of blast-resistant projects. However, previous works have mainly concentrated on the mechanical behavior of materials or plane geometry structural systems. The performance of curved rubber-reinforced concrete panels under near-field blast loads is still a grey area [19]. The objective of this paper is to address this void using a thorough numerical study of the effect of the rubber content and the degree of curvature on failure patterns and the blast resistance of the reinforced concrete barrier walls [2], [13].

WORK OBJECTIVE

Despite the research that was already performed on rubberized concrete and its behavior under dynamic and blast loading, there is still a notable gap to be filled in the literature about the structural performance of the blasted rubber-reinforced concrete (RRC) curve configurations. The majority of the earlier studies have shown an interest in the flat shape while leaving the potential of the curved configuration largely untapped. Responding to the need for further research, this work will present an elaborate numerical study that describes how the conversion of the geometry of concrete walls from flat to curved affects both the incident overpressure and the resulting structural damage under explosive loading in detail.

This study is initiated by the comparison of four finite element models with the results of the blast test, whose origin is experimental. The rubber compositions represented by the models under consideration are 0%, 10%, 30%, and 50%, respectively. The accuracy of the numerical simulation framework and the dependability of the outcomes can be ensured by this stage [7].

Next, the study presents a set of eight advanced numerical models and their results that were generated by the analysis of these models to show the change of shape of the wall from flat to curved and the various angle variations of curvature, on the wall that was tested for the blast, failure patterns, and the distribution of stress. The research is a comprehensive discussion of how the curvature dynamically cooperates with the material to improve the overall security performance of barrier structures against the influence of the blast.

Numerical Modelling

Given the high cost and stringent safety requirements associated with full-scale experimental testing under blast conditions, numerical modeling emerges as an indispensable alternative for investigating the

response of structural systems to explosive loads. Finite Element Analysis (FEA) offers a robust platform to simulate such high-energy events with precision and control. In this study, advanced numerical simulations were carried out using the ABAQUS software suite [20], which is widely recognized for its comprehensive capabilities in modeling nonlinear dynamic behavior and blast-structure interaction [16].

This work presents the theoretical framework, computational methods, and material models used to simulate the response of rubber-reinforced concrete (RRC) barrier walls under blast loading scenarios. This numerical approach allows for detailed analysis of stress distribution, failure mechanisms, and energy dissipation with high accuracy, offering valuable insights into the structural behavior of RRC during extreme loading conditions.

Modal Validation

This section delineates the affirmation stage for the rubberized concrete flat slabs under the action of steel reinforcement. The numerical models are instantiated to carry out this process, and [25] have conducted an experimental investigation as a source of experimental evidence. There are four such blast tests to be Conducted: Each slab has been made to vary in the percentage of rubber particles and the. concrete mix used. The trials of the rubberized concrete slabs in the blast situation were tested as follows: 0% (NC), 10% (RC10), 30% (RC30), and 50% (RC50). Each specimen was of uniform size 2000 mm × 2000 mm × 100 mm, held together by both the upper and lower steel meshes with a frequency of 8 mm diameter bars spaced at 200 mm intervals, which corresponded to a reinforcement ratio of μ = 0.251%. The basic details of reinforcement are demonstrated in Figure 1.

Regarding the experiment setting, the slabs under the condition of a detonation of 560 grams of the ANFO explosive (ammonium nitrate-fuel oil) at a distance of 0.50 meters above the slab surface, as visualized in Figure 2. The steel whose mechanical properties were built into the various experimental setups was supposed to have a yielding strength of 235 MPa and Young's modulus of 210 GPa.

To simulate the same event in a virtual environment, dynamic geometrically nonlinear analyses were carried out using the finite element software ABAQUS (20). This tool SN, provided the opportunity to use high-quality models to visualize the transition of the blast wave and the dynamics of the structural response under extreme loads. As a result, through simulations, the accuracy and the predictive ability of the finite element models were experimentally confirmed before their usage in the extension of the parametric studies in the future chapters.

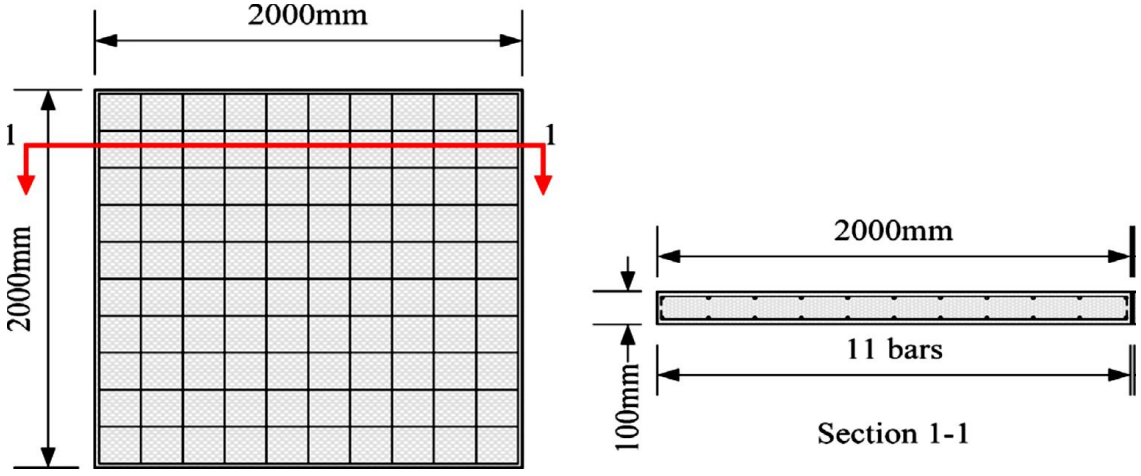

Figure 1. Slab's dimensions and reinforcing [14].

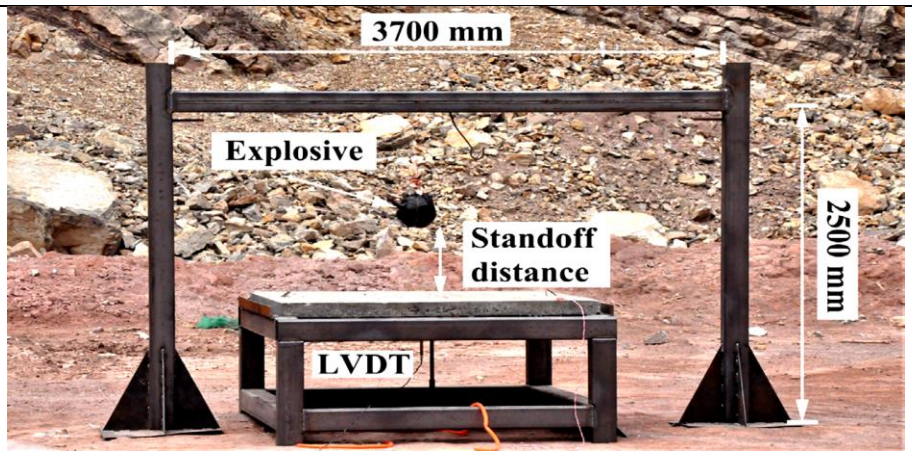

Figure 2. Picture showing the system being used for field testing (25).

Working with reinforced concrete requires specialized skills. Consequently, it is required to develop a finite element model that can predict concrete's elastic and plastic behavior in tension and compression. Compression, crushing, and tensile cracking are two key elements that affect CDP behavior. Table 1 displays the material's properties. The stress-strain curves of all four types of concrete are given in Fig. 3. The parameters for the CDP model are summarized in Table 2 [22].

The Data defines the stress-strain curve of RC30 in tension given in Table [3]. Data defines the stress-strain curve of RC30 in compression, given in Table [4].

Table 1. Data defines the used material [14].

	$f_c(MPa)$	$f_t(MPa)$	$E_c(GPa)$	ν
NC	34.91	3.06	25.85	0.21
RC10	32.58	3.04	24.28	0.19
RC30	27.93	3.00	22.78	0.19
RC50	24.63	2.43	19.70	0.19

Table 2. Parameters of the CDP model for NC, RC10, RC30 and RC50.

Concrete Type	Dilation angle (ψ)	Eccentricity(e)	Shape parameter (Kc)	Maximumcompression axial/biaxial (fbo/fco)	Viscosity(μ)
NC	35	0.1	2/3	1.16	0
RC10	40	0.1	2/3	1.16	0
RC30	38	0.1	2/3	1.16	0
RC50	38	0.1	2/3	1.16	0

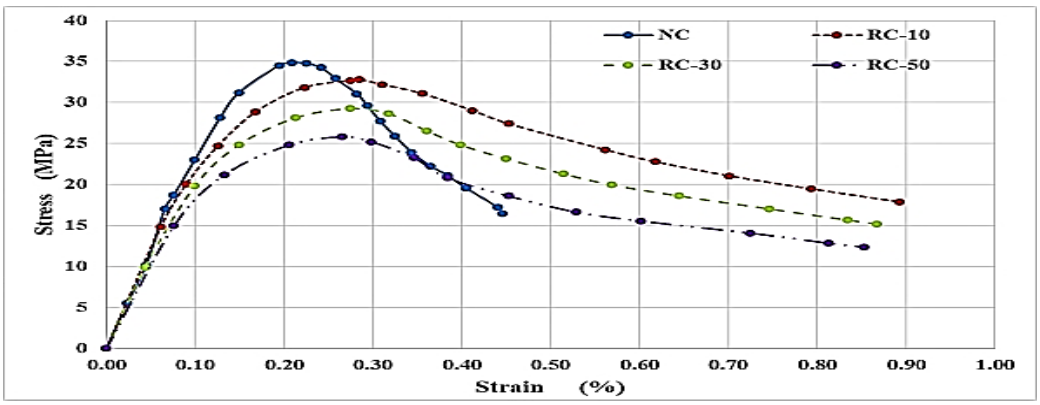

Figure 3. Stress-strain curve for all types of concrete

Table 3. Data defines the RC30 in tension.

Stress σt (N/m2)	**Strain (ε)**	**Elastic Strain (εel)**	**Plastic strain (εpl)**	**Damage parameter (dt)**
0	0	0	0	0
3.40E+06	1.50E-04	1.50E-04	0.00E+00	0
1.96E+06	3.60E-04	8.65E-05	2.74E-04	4.24E-01
1.61E+06	6.10E-04	7.10E-05	5.39E-04	5.26E-01
1.43E+06	0.001	6.31E-05	9.37E-04	5.79E-01
1.16E+06	0.002	5.14E-05	1.95E-03	6.58E-01
1.04E+06	0.003	4.59E-05	2.95E-03	6.94E-01
9.30E+05	0.004	4.10E-05	3.96E-03	7.26E-01
8.10E+05	0.005	3.57E-05	4.96E-03	7.62E-01
7.10E+05	0.006	3.13E-05	5.97E-03	7.91E-01

Table 4. Data defines the RC30 in compression

Stress σc(N/m2)	**Strain (ε)**	**Elastic strain (εel)**	**Plastic Strain (εpl)**	**Damage parameter (dc)**
0.00E+00	0.00E+00	0	0.00E+00	0
9.91E+06	4.35E-04	4.35E-04	0.00E+00	0
1.98E+07	9.95E-04	8.70E-04	1.24E-04	0
2.48E+07	1.49E-03	1.09E-03	4.02E-04	0
2.81E+07	2.13E-03	1.24E-03	8.96E-04	0
2.92E+07	2.75E-03	1.28E-03	1.46E-03	0
2.86E+07	3.17E-03	1.26E-03	1.92E-03	2.09E-02
2.66E+07	3.60E-03	1.17E-03	2.43E-03	9.21E-02
2.48E+07	3.98E-03	1.09E-03	2.89E-03	1.51E-01
2.31E+07	4.50E-03	1.02E-03	3.48E-03	2.09E-01
2.13E+07	5.14E-03	9.35E-04	4.20E-03	2.72E-01
1.99E+07	5.68E-03	8.76E-04	4.81E-03	3.18E-01
1.86E+07	6.44E-03	8.17E-04	5.63E-03	3.64E-01
1.70E+07	7.46E-03	7.47E-04	6.71E-03	4.18E-01
1.57E+07	8.34E-03	6.88E-04	7.65E-03	4.64E-01
1.52E+07	8.67E-03	6.66E-04	8.00E-03	4.81E-01

Finite element model

For the finite element in this model used in the present work, the rubber-reinforced concrete slab was meshed employing two different element types via the information in Table 5. The domain of the concrete was considered by C3D8R elements (hourglass control and full integration). The benefit of using these is that they are good for capturing 3D nonlinear dynamic deformation behavior, Zienkiewicz et al. [22]. The longitudinal steel bars, however, were simulated by T3D2 elements that exhibit 2-node, 3D trusses, which are capable of accurately representing the axial behavior of the steel reinforcement bars embedded within the concrete matrix.

Both computational efficiency and numerical accuracy were achieved by conducting a mesh convergence study. As per the results, a mesh configuration with an element size of 10 mm used for all simulation cases was the best choice. This mesh resolution was the most suitable choice for completing the problem with an adequate level of precision and used the least amount of time. This mesh size selection is in line with existing numerical studies where mesh convergence analysis demonstrated that 10 mm elements provide a good balance between computational demand and solution accuracy for dynamic RC slab simulations [23]. For instance, the work of Elmenshawi et al. (2020) conducted a detailed parametric study on mesh sensitivity and recommended similar mesh densities for nonlinear simulations of reinforced concrete under blast loads, ensuring that critical stress localization and crack propagation are not underestimated. The illustrated dense mesh in Fig. 4, along with the geometric representation of the reinforced slab, provides a visualization of where the reinforced slab is and how

the elements and reinforcement are distributed. The diagram shows the elements fixed at the four corners of the slab and the alignment of the nets with the loaded surface. Due to the combination of this meshing strategy with the chosen element types, the model became capable of fully capturing all the material and interaction behaviors of the reinforced concrete slab under blasted conditions, guaranteeing that both the structural and interaction types of the model throughout the operation of the simulation were valid [8] [23].

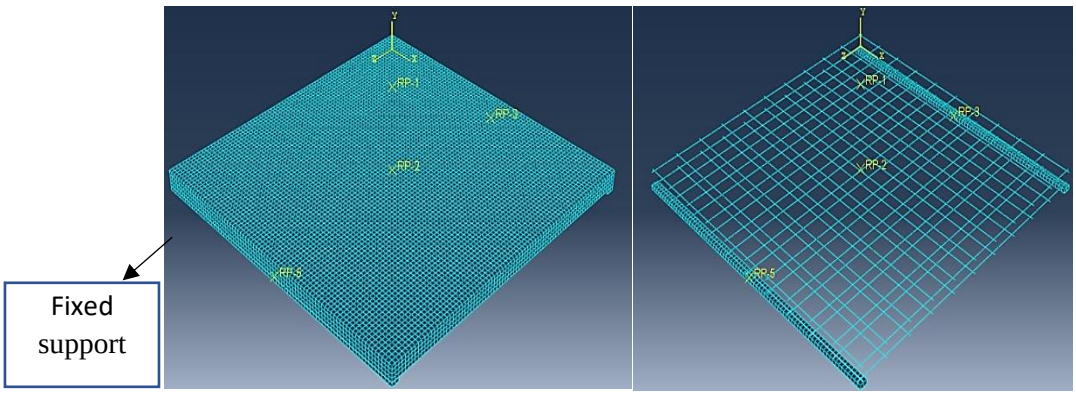

Figure 4. Finite element mesh

Table 5. Types of finite elements used in numerical simulation.

Description	Type	Part
8-node linear brick with hourglass control	C3D8R	Concrete Slab
2-node, three-dimensional truss element	T3D2	Longitudinal Steel

A combination of ABAQUS [13] and CONWEP (Conventional Weapons Effects Program) air-blast model is chosen that closely represents the real-life conditions. This streamlining can express blast wave pressure as a function of both time and space created from published blast wave data that does not require the modeling of explosive detonation and air domain explicitly.

This numerical investigation focused on applying blast loads to a concrete slab, utilizing the CONWEP approach within ABAQUS. The selection of CONWEP was primarily driven by its computational efficiency and ease of implementation, given its reliance on empirical pressure-time histories derived from experimental data. This method allows for rapid simulation of blast effects without the need for complex fluid-structure interaction modeling, making it well-suited for large-scale structural analyses where detailed wave propagation and reflection phenomena are not critically emphasized. In comparison, Arbitrary Lagrangian-Eulerian (ALE) methods and explicit air models offer more accurate simulation capabilities for shock wave propagation and reflected wave interactions, capturing complex wave dynamics and nuanced pressure variations. However, these approaches are computationally intensive, requiring extensive meshing, longer simulation times, and more elaborate setup procedures. In the experimental phase, the effect of blast pressure was studied without accounting for reflected waves. Accordingly, the choice of CONWEP in ABAQUS was appropriate for replicating the primary blast load while simplifying the analysis by neglecting the complex reflected wave phenomena [29].

The air blast source in the simulation environment was configured in the interaction property module, which was implemented by the definition of the incident wave according to the most important parameters in Table 6. In the model setup, the explosive, which was used in the experiment, was ammonium nitrate fuel oil (ANFO) that was represented as the same mass of trinitrotoluene (TNT), with a percentage of 0.88, which was a good fit with the equivalence scale. In the validation tests, the blast imitation was generated by a TNT mass of 4.928 kg. This technique of simulation was efficient in computational terms and as a means of reproducing the pressure wave delivered just right and, therefore, providing the interaction sequence with the wall, which was consistent with the experiments and ensured computational efficiency of simulations.

Table 6: The definition of the incident wave

Definition	Conweb
Wave Property	Air Blast
Scale Factor	1
Equivalent Mass of TNT	4.928kg (TNT)

Numerical Results

As illustrated in Figure 5, the shape of the damage in the experimental test for the RC30 slab is compared to the shape of the damage in the numerical simulation. The failure of concrete was evaluated using a combination of principal stress analysis, strain criteria, and damage metrics within the framework of the Concrete Damage Plasticity (CDP) model. Specifically, the principal stresses and strains were monitored to identify the onset of cracking and failure. Additionally, the damage variable provided by the CDP model was used to quantify the deterioration in material integrity, following the conventional approach to CDP modeling as described in the literature. This method allows for a comprehensive assessment of concrete failure, capturing both the initiation and progression of damage based on the evolution of stress, strain, and damage parameters in accordance with established practices.
The stress component S33 and the corresponding damage progression are presented simultaneously in the same figure, illustrating the effects of increasing the tensile strength of the concrete.

Figure. 5. Damage at failure of RC30 slab

As seen in the previous picture, there is excellent agreement between the experimental model and the given F.E model on the manner of failure. The failure mechanisms and peak mid-span deflections for the slab specimens subjected to blast load are compared in Table 7 using experimental and numerical analysis. As can be observed, there is a mean difference of 4.3% between the experimental and numerical peak deflections, indicating generally good agreement.

Table 7. Experimental and verified F.E model results

Slab Number	Permanent deflection(mm)		Mid-Span Failure		Def.
	Experimental	Numerical	Experimental	Numerical	Exp./Num.
NC	149	142	Tensile failure	Tensile failure	1.047%
RC10	122	116	Tensile failure	Tensile failure	1.05%
RC30	150	143	Tensile failure	Tensile failure	1.048%
RC50	157	152	Tensile failure	Tensile failure	1.03%
			Mean		1.043%

The overpressure obtained from the test of two different samples of the experimental test was also compared to numerical analysis, as shown in Fig. 6. It is clear that experimental and numerical overpressures generally accord well.

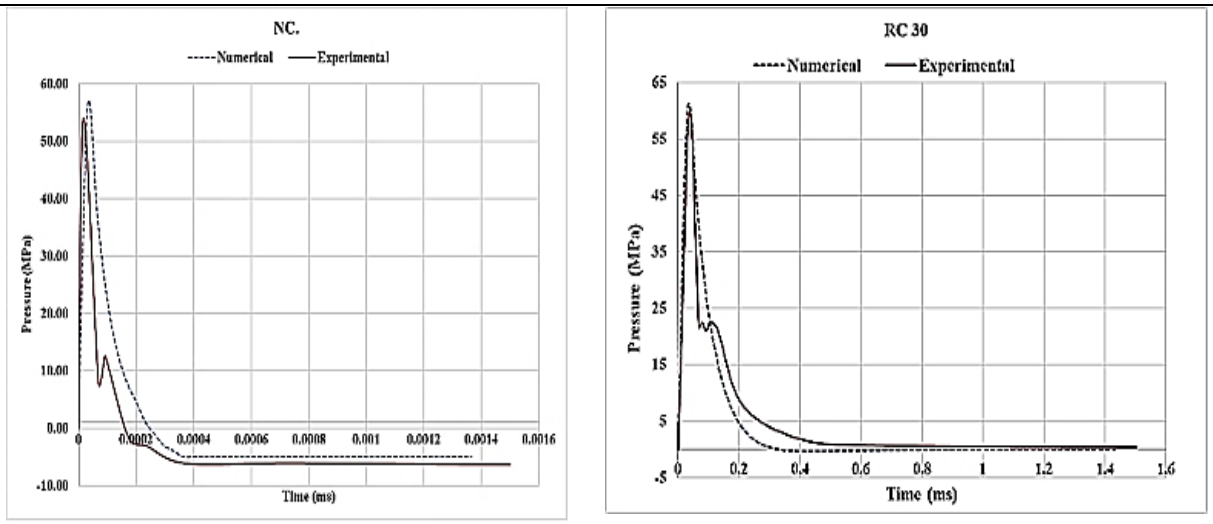

NC. (0.282 m/kg3) RC30 (0.282 m/kg3)

Figure 6. Overpressure Histories at the center of slabs

Proposed Structural Configuration

The modified form proposed in this research paper includes a bent rubber-strengthened concrete barrier wall designed to study the impact of geometric curvature on blast resistance. In the near-field detonation of the realistic simulated explosion, the wall is affected by the explosion of 560 grams of ammonium nitrate fuel oil (ANFO) of intermediate explosive strength, corresponding to a standoff distance of 0.5 meters from the wall's front face. The primary purpose of this blast wave is to find out the curvature effect in that aspect where the wave is not so intense, and the strength of the damage has been partly neutralized. According to Fig. 7, the discussed barrier design is presented as geometrically identical to the already validated reference model in terms of dimensions, reinforcement types as well as quantities, i.e. 2000 mm × 2000 mm × 100 mm with a single, equal to 2.44, reinforcement ratio. However, the change is visible through the shape of the wall only, where the authors have considered three curvature configurations: 0° (flat), 23°, and 48°. The given deviations from the previous shape are chosen to enable the experiments, which are to analyze in an arranged manner the influence of curvature with reference to the load dynamic, the stress distribution, and the failure features under explosive loading. This design approach allows making comparison tests in order to study the difference between flat and curved shapes and in this way, to understand in depth how the curvature can be a significant factor in improving the blast resistance of rubberized concrete structures.

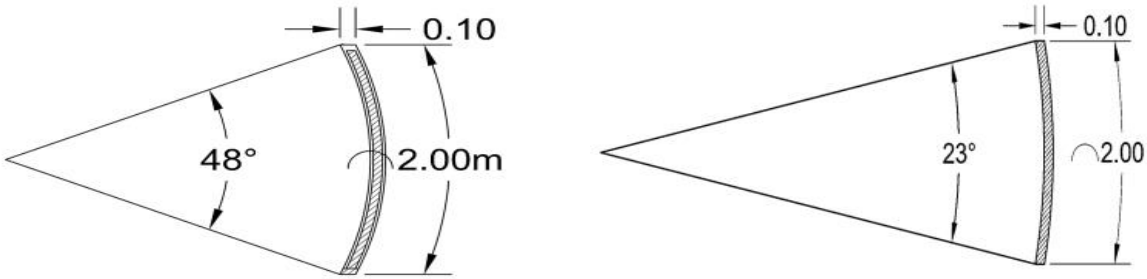

Barrier wall angel (480) Barrier wall angle (230)

Figure 7. Dimensions of a concrete barrier wall

Finite Element Model

The structural model of the proposed curved rubber-reinforced concrete (RRC) barrier wall was discretized by numerical means using two element types that were aligned with the ones used in the validation process. For the concrete region, C3-D8R elements were prepared, which are eight-node linear hexahedra with reduced integration and hourglass control that accurately represent the material

behavior and response under some blast-induced conditions. Also, T3-D2 elements representing the embedded steel reinforcement were utilized, the 3D two-nodded truss elements that are suitable for the axial behavior of the reinforcing bars in the concrete.

To guarantee that all the tasks are carried out with a high numerical accuracy and that all models are computationally stable, a mesh convergence study was conducted. As a result, a 10 mm-based fine mesh was chosen for all the simulations. It is this fine mesh resolution that will allow the model to capture stress gradients and crack propagation processes in a better way, especially in highly stressed and curved geometries.

The configuration of the final finite element mesh is given in the form of Figure 8, in which we can see a visually well-disposed assortment of elements and an evenly distributed density of elements. Furthermore, Figure 9 offers a detailed layout of the reinforcement as well as the final shape of the curved slab, thereby proving also the fact that the reinforcement ratio is consistent with that of the validated flat model. Therefore, this strategy of modeling is an approach that, in all the areas of change in structural performance, the only factor that can be accounted for is geometric curvature. Therefore, it allows for deep analysis of blast mitigation through the change of the geometry only.

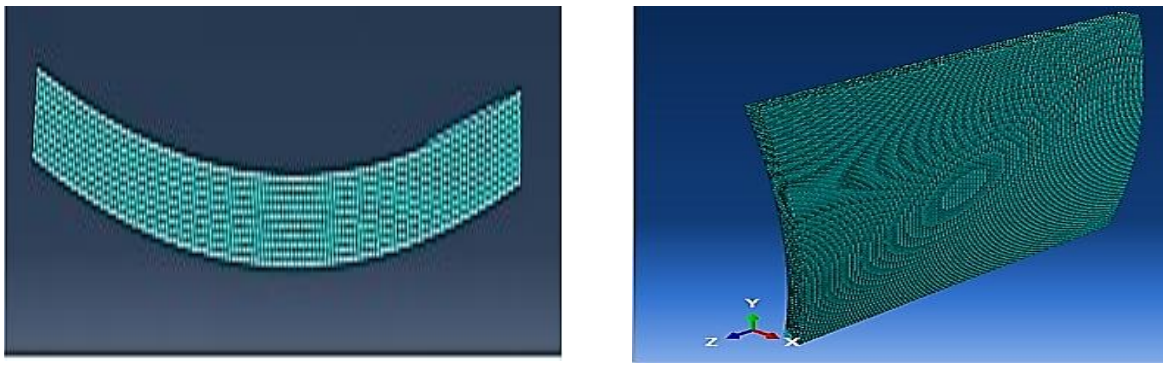

Figure 8. Finite element mesh

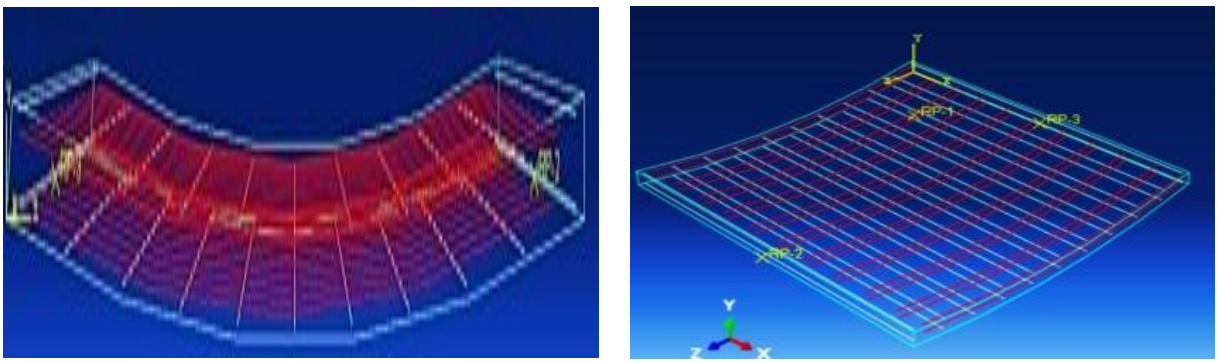

Figure 9. Model geometry

NUMERICAL RESULTS AND DISCUSSION

This section outlines a thorough examination of the influence of curvature angle on the structural response of both rubberized and plain concrete barrier walls when they receive blast loading. In order to only analyze the impact of curved barrier geometry, the slabs of the geometric and reinforcement parameters were kept unchanged in all the models. These curves of 23° and 48° angles were selected to represent the transition from flat slab to structural profiles with a curved configuration, thus verifying the persistence of the concrete volume and the steel section. Thus, it is simple and straightforward to find out how the movement of the curvature angle causes restriction or flexion on the main parameters such as overpressure distribution, stress level, the extent of deformation, and failure mechanisms of a given barrier. The results make a significant contribution to the knowledge of wall shape to the impact resistance of different concrete types in the event of a blast.

Overpressure

To study the blast performance of the proposed barrier configurations, the highest overpressure at the front face of each slab was calculated from the pressure–time history curves obtained by numerical simulation. A comparison of the flat model, which was validated before, and the new curved models, focusing on three main features: the overpressure, the deflection, and the mode of failure, was then performed. The determined values of the peak pressure and the corresponding deflection of all researched configurations are listed in Table 8.

The effect of the curvature on the overpressure decrease was evaluated at first in each of the four concrete types—NC (normal concrete), RC10, RC30, and RC50. According to the data presented in Figure 10, the overpressure has decreased to a greater extent as the degree of the curvature angle was increased for all the types of concrete. More specifically, the results for the NC slab showed that the overpressure was first been reduced from 60.05 MPa for the flat configuration (0°) to 55.55 MPa at 23° of curvature, and then to 50.05 MPa at 48° of curvature. These data obviously prove that the slab's blast pressure dissipation capability is improved as the slab becomes more curved, through a geometrical transformation used for design, which is also not considered in the presence of rubber.

Table 8. presents the peak pressure and deflection recorded at the middle point of slab

No.	Verified model		Proposed model with angle (230)		Proposed model with angle (480)	
	Peak overpressure (MPa)	Deflection (mm)	Peak overpressure (MPa)	Deflection (mm)	Peak overpressure (MPa)	Deflection (mm)
NC	60.05	140	55.55	152.7	50.05	173
RC10	59.6	116	52.34	138	48.05	168
RC30	58.3	143	49.23	153	40.78	172.3
RC50	51.5	152	46.06	158	38.6	180

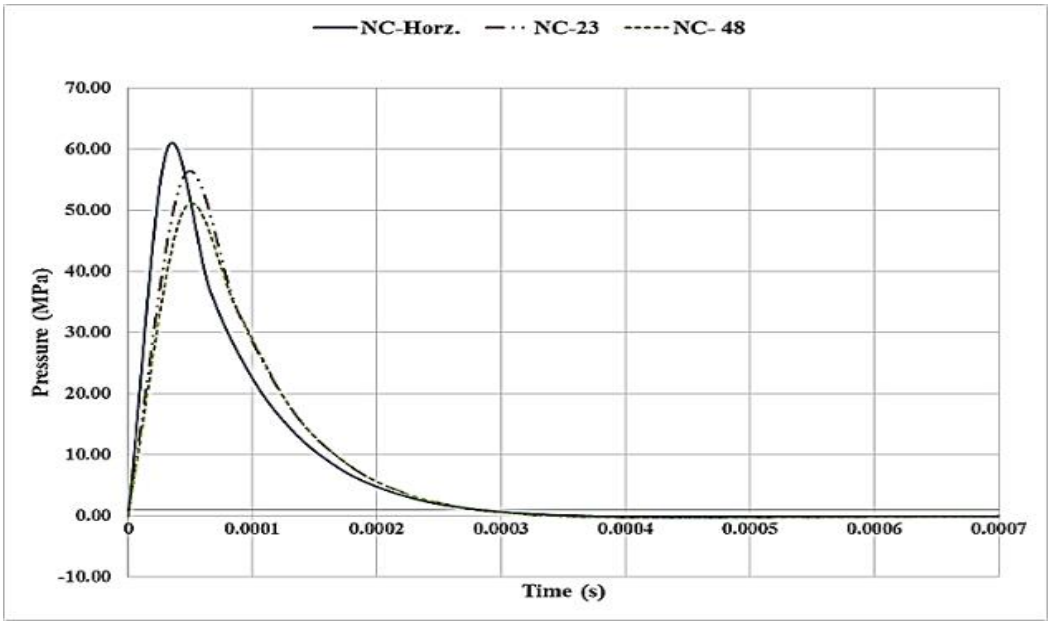

Figure 10. Overpressure at various angles of the NC slab

After that, the effect of the change of curvature angles on the overpressure of the RC10 model was studied. There was also observed a change in the overpressure values to the lowest as a result of increasing the angle of curvature from zero to 480, as shown in Figure 11.

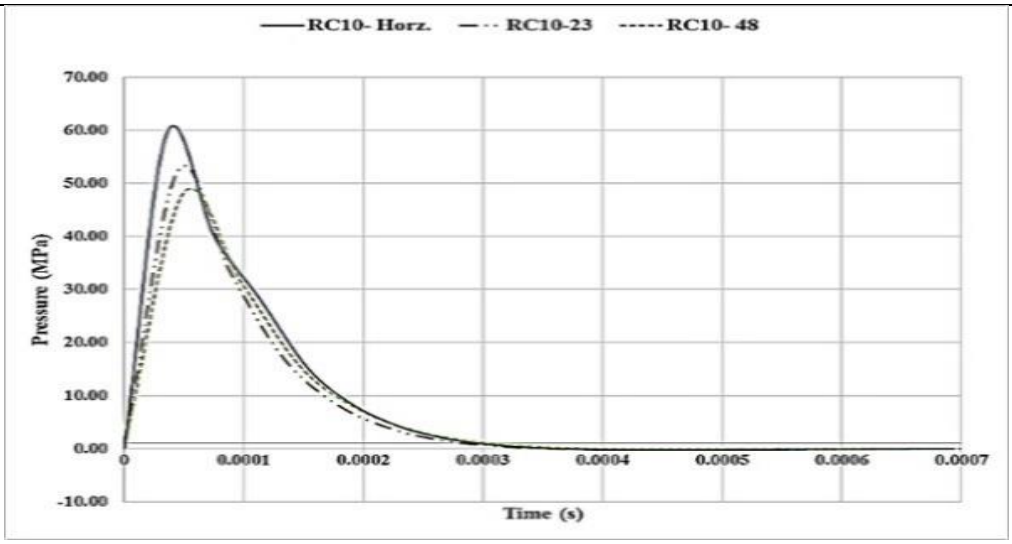

Figure 11. Overpressure at various angles of RC10 slab

The study was also done on RC30 and RC50, and a decrease in overpressure was observed with the increase in curvature angle, as shown in Figure 12. and Figure 13.

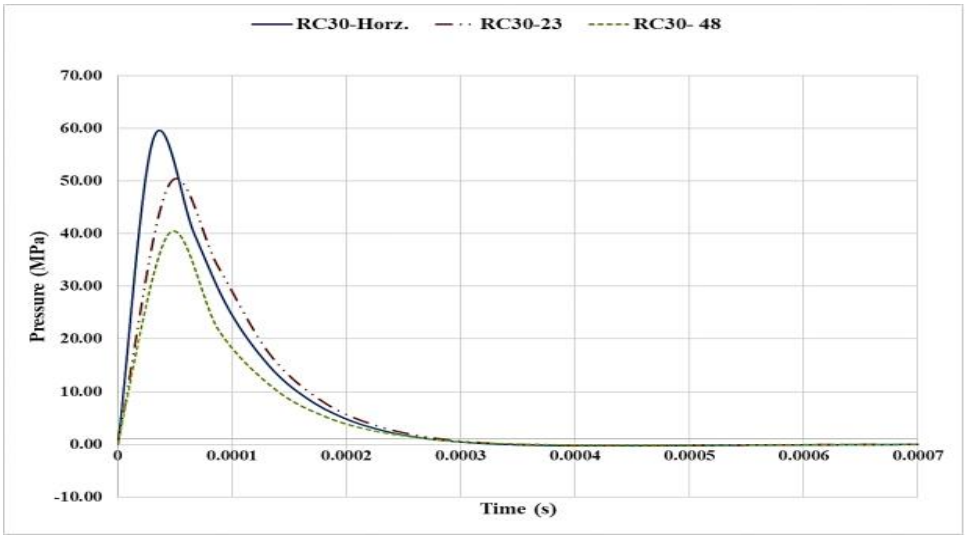

Figure 12. Overpressure at various angles of RC30 slab

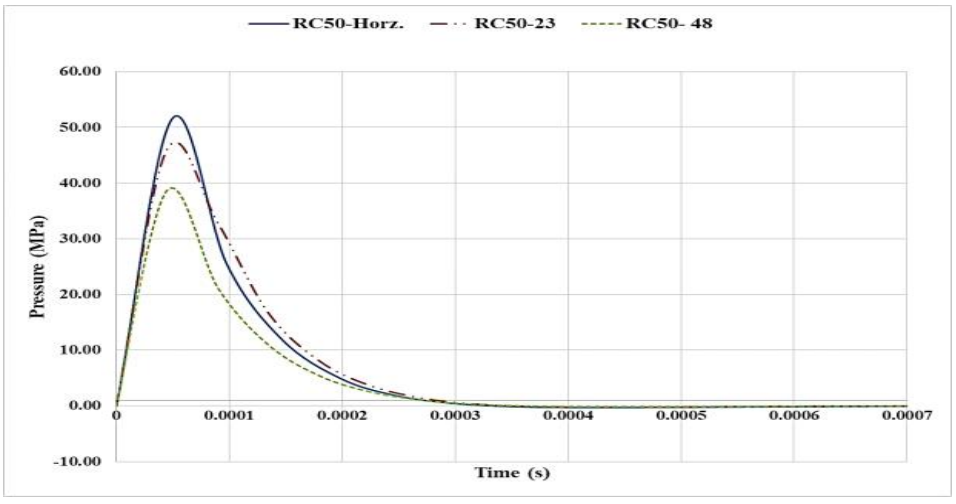

Figure 13. Overpressure at various angles of RC50 slab

Mode of Failure

The second parameter analyzed is the collapsed form of the different slabs due to blast waves. The shape of damage to a normal concrete barrier wall with different angles of curvature is shown in Figure 14.

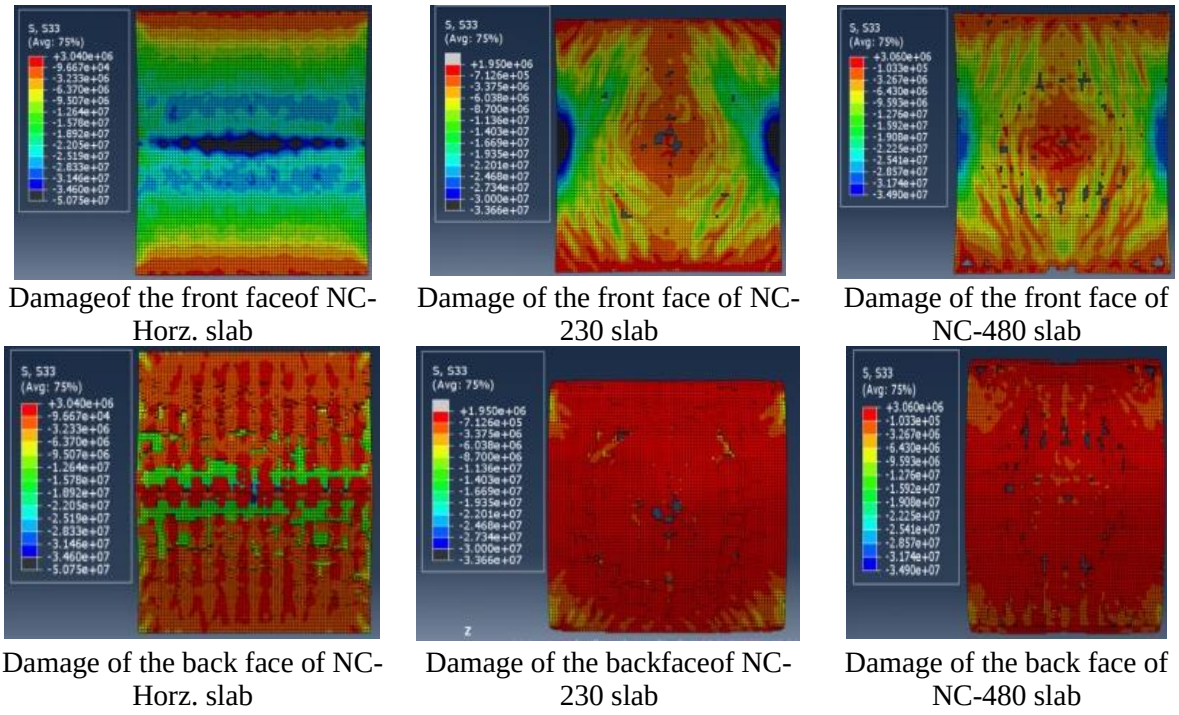

Damageof the front faceof NC-Horz. slab | Damage of the front face of NC-230 slab | Damage of the front face of NC-480 slab

Damage of the back face of NC-Horz. slab | Damage of the backfaceof NC-230 slab | Damage of the back face of NC-480 slab

Figure 14. Comparison between failure modes of NC-Horz., NC-230and NC-480slab at 45 Ms

The most severe structural damage, as shown in Figure 14, occurred in the flat normal concrete slab (NC-Horz), whereas the slab with 48° curvature (NC-48) demonstrated the least extent of collapse, as a direct visual comparison of the failure modes under equal simulation time step. Under the flat NC arrangement, the compressive stresses at the front of the slab were too high compared to the material's limit, and the result was a significant crushing event. In this process, the tensile forces were generated on the front face, and the rear failed under high tensile stress, thus constituting significant cracking and separation of the concrete surface.

It can be seen that the initial moderate curvature reduced the severity of the slabs' in-plane. The stress was concentrated at the parts of the slab that took the shape of the crack, whereas the central portion of the front stayed within the compression stress field limit. The impact was localized, and the slab was found to be penetrated slightly there. On the rear face, the failure process resembled the flat slab except that it occurred at a higher stress level.

opposite reasoning, the NC-48 slab was a very clear example of how stress acquires a very good distribution. The compressive stresses at the edges were small, whereas the penetration in the center was very low. All these conclusions come to the point that by increasing the curvature angle, the capacity of the slab to accept the blast energy will elevate significantly, resulting in a more controlled and less destructive failure pattern.

Nonetheless, with the extremely highly curvature sets of slabs, the only consistent damage observed was localized failure at the end regions, implying that as the curvature increased, the slab ends became localized failure points. Therefore, with high curvature slabs, the addition of stiffness (by either thickening the cross-section or increasing the reinforcement ratio) should help eliminate or at least minimize localized failure at the end regions to prevent premature collapse. In considering the RC10 slabs, the failure behavior noted for those slabs was consistent, whereas the only difference appeared to be that the RC10-23 configuration had a slightly increased penetration zone depth at the center. This leads the author to conclude that while the addition of rubber contributes to energy absorption, the

addition of rubber, when combined with moderate curvature slabs (especially with lower rubber content), can also affect local resistance to blast response. The detailed damage profiles for the RC10 slabs are in Figure 15.

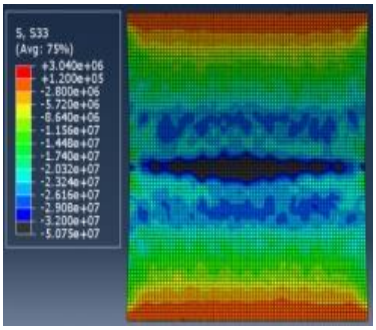

Damage of front face of RC10-Horz. slab

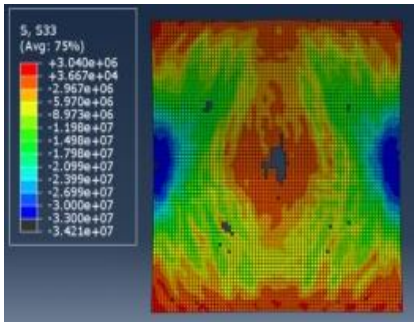

Damage of front face of RC10-230 slab

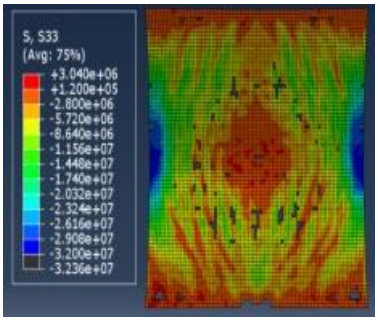

Damage of front face of RC10-480 slab

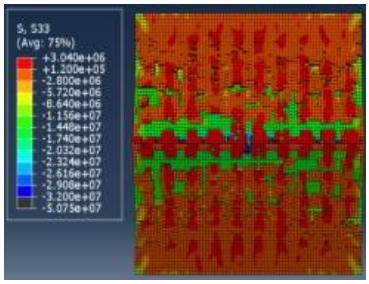

Damage of back face of RC10-Horz. slab

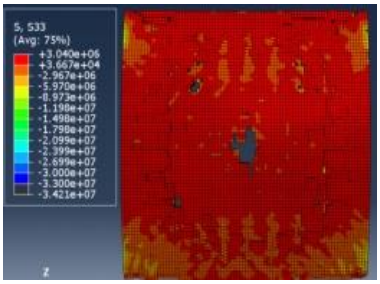

Damage of back face of RC10-230 slab

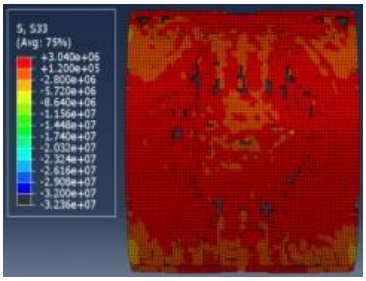

Damage of back face of RC10-480 slab

Figure 15. Comparison between failure modes of RC10-Horz., RC10-230, and RC10-480 slab at 45 ms

In the study of the failure behavior of the RC30 slab, the effect of curvature angle was once again observable, as shown in Figure 16. It might be noted that the overall pattern of the collapse was similar to that of the RC10 slab; however, there was a clear difference in the amount or level of failure at different levels of curvature. The RC30 slab with a curvature angle of 23° exhibited more damage near the ends and exhibited localized collapse, which was likely an effect caused by redistributing stress toward the ends of the slab. The RC30 slab with a curvature angle of 48° allowed less area of the slab ends to be affected, and thus, this width of damage indicates a more desirable flow of stress and better performance of structural action in response to the blast loading. This evidence further supports the finding that curvature can aid in the distribution of energy and can allow for less damage to the mid-span, although it could also induce edge vulnerability if not mitigated. Using either a convex or concave curvature geometry loaded with sufficient curvature warrants reinforcing the ends of the slab by either increasing the depth of the cross-section or adding reinforcement, in order to avoid localized failure.

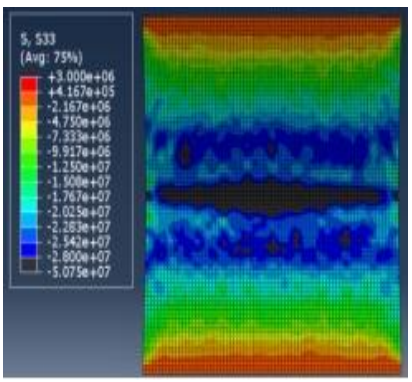

Damage of front face of RC30-Horz. slab

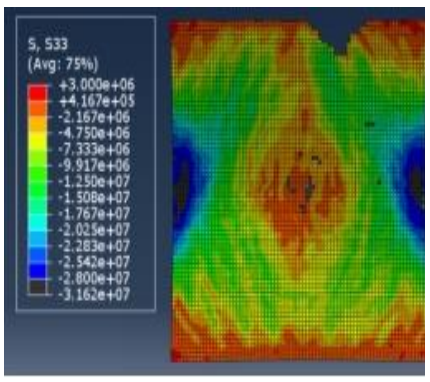

Damage of front face of RC30-230 slab

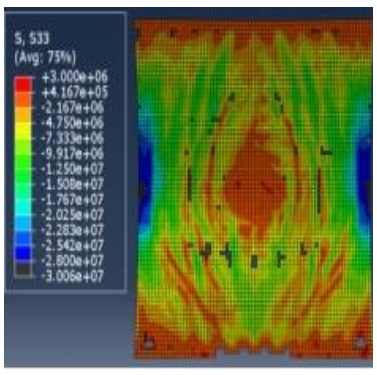

Damage of front face of RC30-480 slab

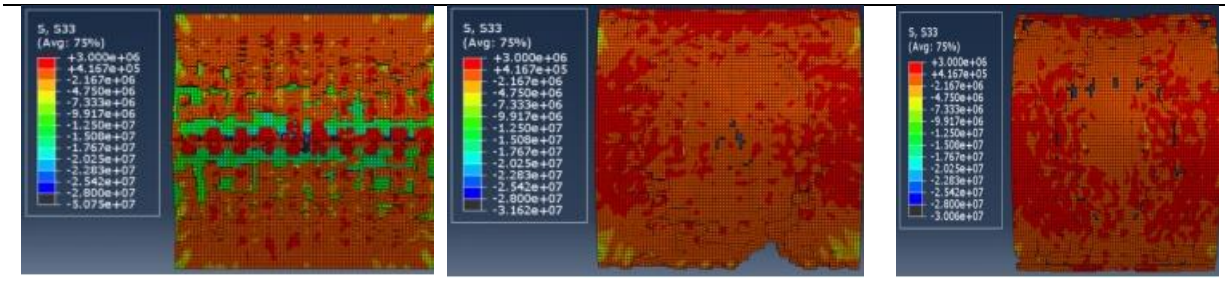

Damage of back face of RC30-Horz. slab | Damage of back face of RC30-230 slab | Damage of back face of RC30-480 slab

Figure 16. Comparison between failure modes of RC30-Horz., RC30-230 and RC30-480 slab at 45 ms

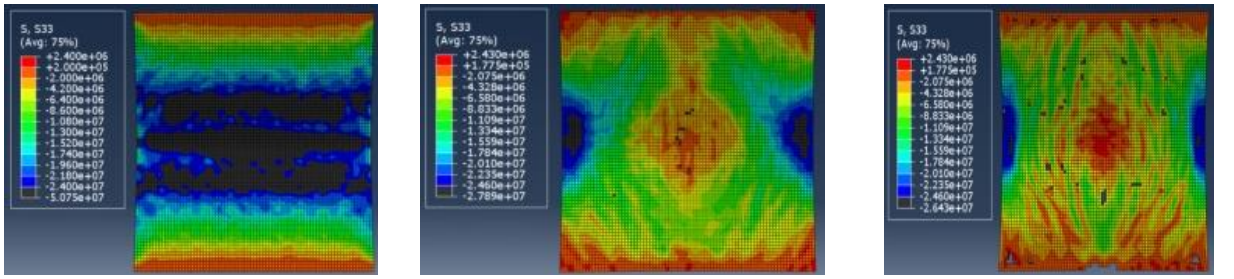

Damage of front face of RC50-Horz. slab | Damage of front face of RC50-230 slab | Damage of front face of RC50-480 slab

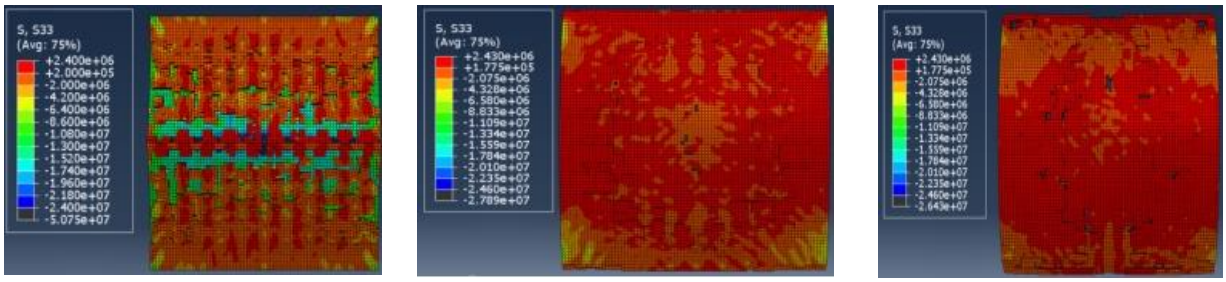

Damage of back face of RC50-Horz. slab | Damage of back face of RC50-230 slab | Damage of back face of RC50-480 slab

Figure 17. Comparison between failure modes of RC50-Horz., RC50-230 and RC50-480 slab at 45 ms

As shown in Figure 17, What sets the RC50 slabs apart from the other slabs is that they have an overall lower percentage of collapsed areas when compared to slabs with lower rubber content. Although the flat RC50 slab had significantly more damage than the curved slabs, the total volume of failures was still less than that of the NC, RC10, and RC30 slabs. This indicates that a high proportion of rubber particles (up to 50% as a partial substitute for sand) improves the performance of the slab and its ability to absorb and redistribute blast energy when combined with a curved geometry. Therefore, it appears that rubberized concrete with high percentages of rubber (50%) and a curved slab may be an effective measure to resist blasts and minimize collapse approximately the area of localized failure under explosive loads.

CONCLUSIONS

The study examined the use of rubberized concrete for curved barrier wall systems that protect against the destructive effects of blast (blast load) with an emphasis on decreasing overpressure and reducing failure. A proliferation of nonlinear numerical models was conducted utilizing the ABAQUS software platform, specifically a three-dimensional hydrocode model previously corroborated through experimental data found in published papers. The results yielded valuable information regarding the relationship between wall curvature, rubber content, and blast resistance. Based on the findings of this research, the following conclusions can be drawn:

The developed finite element model demonstrated a strong correlation with experimental results, affirming its reliability for further parametric investigations involving blast-resistant design.

Compared to flat slabs, all of the curved walls were consistently more effective at reducing peak overpressure and limiting structural damage across all performance based-off the variations tested.

In normal concrete (NC), the peak overpressure measured for the flat configuration was 60.05 MPa. The peak overpressure for the flat slab with a 23° curvature was 55.55 MPa, and with a 48° curvature it was 50.05 MPa. This shows that there was a positive effect of geometric transform on blast performance.

For RC10 slabs, with the variable of 48° curvature, there was a reduction of 19% peak overpressure compared to the flat version. This seems like a moderate improvement in blast mitigation.

RC30 and RC50 slabs with a higher rubber content showed an even bigger reduction in peak overpressure, 30% and 25%, respectively, when changing from flat to a 48° curved version was performed.

In all of the four concrete types (NC, RC10, RC30, RC50), the 48° curvature configuration provided a relatively uniform stress distribution on the front face of the curved structure with trends of the lowest edge stresses and least mid-span penetration compared to the stresses achieved at 23° curvature.

Improved curvature can increase blast resistance, but simulations have shown that slabs with large curvature angles could fail locally at the ends, caused by stress concentration and stiffness discontinuities at the ends.

In cases like this it is suggested to strengthen the ends of slabs, in a highly curved configuration, by increasing sectional thickness or the reinforcement ratio, so collapse will not happen too early. This will allow for structural continuity in the event of an explosion.

The results of using rubber particles in concrete, particularly with an optimally curved geometry, provide an efficient method to enhance blast resistance for protective structural systems. These findings provide excellent design guidelines for civil or military infrastructures subjected to blast threats [5] [21].

REFERENCES

[1] Feng W, Tang Y, He W, Wei W, Yang Y. Mode I dynamic fracture toughness of rubberised concrete using a drop hammer device and split Hopkinson pressure bar. Journal of Building Engineering. 2022 May 1; 48:103995. https://doi.org/10.1016/j.jobe.2022.103995

[2] Kara De Maeijer P, Craeye B, Blom J, Bervoets L. Crumb rubber in concrete—The barriers for application in the construction industry. Infrastructures. 2021 Aug 20;6(8):116. https://doi.org/10.3390/infrastructures6080116

[3] Lai D, Demartino C, Xiao Y. High-strain rate compressive behavior of fiber-reinforced rubberized concrete. Construction and Building Materials. 2022 Feb 14; 319:125739. https://doi.org/10.1016/j.conbuildmat.2021.125739

[4] Askar MK, Hassan AF, Al-Kamaki YS. Flexural and shear strengthening of reinforced concrete beams using FRP composites: A state of the art. Case Studies in Construction Materials. 2022 Dec 1;17: e01189. https://doi.org/10.1016/j.cscm.2022.e01189

[5] Khalhen IA, Aghayari R. Impact resistance of concrete containing LLDPE–waste tire rubber and silica fume. Journal of Rehabilitation in Civil Engineering. 2023 Feb 1;11(1):60-75. https://doi.org/10.22075/JRCE.2022.23456.1511

[6] Pan L, Hao H, Cui J, Pham TM. Numerical study on dynamic properties of rubberised concrete with different rubber contents. Defence Technology. 2023 Jun; 24:228–40. https://doi.org/10.1016/j.dt.2022.04.007

[7] Tavares RP, Bouwman V, Van Paepegem W. Finite element analysis of wind turbine blades subjected to torsional loads: Shell vs solid elements. Composite structures. 2022 Jan 15; 280:114905. https://doi.org/10.1016/j.compstruct.2021.114905

[8] Pei TY, Mokhatar SN, Mutalib NA, Hakim SJ. Numerical Simulation of Modified Rubberized Concrete Block Under Impact Loads. InIOP Conference Series: Materials Science and Engineering 2021 Nov 1 (Vol. 1200, No. 1, p. 012022). IOP Publishing. https://doi 10.1088/1757-899X/1200/1/012022

[9] Li D, Xiao J, Zhuge Y, Mills JE, Senko H, Ma X. Experimental study on crumb rubberised concrete (CRC) and reinforced CRC slabs under static and impact loads. Australian Journal of Structural Engineering. 2020 Oct 1;21(4):294-306. https://doi.org/10.1080/13287982.2020.1809811

[10] Liang C, Fu Y, Wang C, Gao Y, Zhao J. Damping of rubberized recycled aggregate concrete and damping estimation of its elements by finite element analysis. Composite Structures. 2022 Feb 1; 281:114967. https://doi.org/10.1016/j.compstruct.2021.114967

[11] Lai D, Demartino C, Xiao Y. High-strain rate tension behavior of fiber-reinforced rubberized concrete. Cement and Concrete Composites. 2022 Aug 1; 131:104554. https://doi.org/10.1016/j.cemconcomp.2022.104554

[12] Taha AK, Gao Z, Huang D, Zahran MS. Numerical investigation of a new structural configuration of a concrete barrier wall under the effect of blast loads. International Journal of Advanced Structural Engineering. 2019 Dec;11(Suppl 1):19-34.

[13] Taha AK, Gao Z, Dahai H, Zahran MS. Response of a new structural ultra-high performance concrete barrier wall subjected to blast loading. Australian Journal of Structural Engineering. 2020 Apr 2;21(2):154-61. https://doi.org/10.1080/13287982.2020.1719001

[14] Li Y, Zhang K, Lu D, Zeng B. Hydrogen-assisted brittle fracture behavior of low alloy 30CrMo steel based on the combination of experimental and numerical analyses. Materials. 2021 Jul 2;14(13):3711. https://doi.org/10.3390/ma14133711

[15] Otieno J, Wanjiru G. Seismic Innovations: Strengthening Tall Buildings with Advanced Earthquake-Resistant Technologies. Association Journal of Interdisciplinary Technics in Engineering Mechanics. 2024 Sep 30;2(3):18-21.

[16] Senthil K, Gupta I, Rupali S, Pelecanos L. A review on the performance of reinforced concrete structures under blast loading. Journal of Structural Engineering & Applied Mechanics. 2020 Dec 31;3(4):216-28. https://doi.org/10.31462/jseam.2020.04216228

[17] Zhang J, Song X. The AI-assisted traditional design methods for the construction sustainability: A case study of the Lisu ethnic minority village. Natural and Engineering Sciences. 2024 Sep 1;9(2):213-33. https://doi.org/10.28978/nesciences.1569562

[18] Tauma WK, Balázs LG. Impact and blast resistance of slurry infiltrated fiber concrete (SIFCON): A comprehensive review. Concrete Structures. 2023 Dec 17; 24:129-36. https://doi.org/10.32970/CS.2023.1.18

[19] Ariunaa K, Tudevdagva U. Generative Adversarial Network-Based Damage Simulation Model for Reinforced Concrete Structures. International Academic Journal of Innovative Research. 2025;12(2):43-53. https://doi.org/10.71086/IAJIR/V12I2/IAJIR1216

[20] Dede EM, Zhou F, Zhou Y, Lohan DJ, Asheghi M, Goodson KE, Erickson K. Applications, design methods, and challenges for additive manufacturing of thermal solutions for heterogeneous integration of electronics. Journal of Electronic Packaging. 2025;147(2):021009.

[21] Panneerselvam K, Rajendran C. (2025). Development of eco-friendly aquaculture infrastructure using recycled materials. International Journal of Aquatic Research and Environmental Studies. 2025;5(1):577–594. https://doi.org/10.70102/IJARES/V5I1/5-1-54

[22] Zienkiewicz OC, Taylor RL. The finite element method for solid and structural mechanics. Elsevier; 2005 Aug 9.

[23] Choi S, Kim YY. Consistent higher-order beam theory for thin-walled box beams using recursive analysis: edge-bending deformation under doubly symmetric loads. Engineering Structures. 2020 Mar 1; 206:110129. https://doi.org/10.1016/j.engstruct.2019.110129

[24] Shirkoohi ZA. Application of Nanotechnology in the Concrete Industry Improve the Performance of Sustainable Buildings. International Academic Journal of Science and Engineering. 2017; 4(2): 248–256.

[25] Yang F, Feng W, Liu F, Jing L, Yuan B, Chen D. Experimental and numerical study of rubber concrete slabs with steel reinforcement under close-in blast loading. Construction and Building Materials. 2019 Feb 20;198:423-36. https://doi.org/10.1016/j.conbuildmat.2018.11.248

[26] Pan L, Hao H, Cui J, Pham TM. Numerical study on impact resistance of rubberised concrete roadside barrier. Advances in Structural Engineering. 2023 Jan;26(1):17-35. https://doi.org/10.1177/13694332221120130

[27] Zhang C, Gholipour G, Mousavi AA. Blast loads induced responses of RC structural members: State-of-the-art review. Composites Part B: Engineering. 2020 Aug 15; 195:108066. https://doi.org/10.1016/j.compositesb.2020.108066

[28] Şengel H, Özgören A, Erol H, Canbaz M. Mechanical behavior investigation of rubberized concrete barriers in impact load. Challenge Journal of Concrete Research Letters. 2022 Jul 1;13(3):93-100.

[29] Abbood AH. The possibility of accounting measurement of the costs of environmental performance of Iraqi industrial companies: Application study at National Company for Chemical and Plastic Industries 2018-2020. International Academic Journal of Social Sciences. 2022;9(2):102-10. https://doi.org/10.9756/IAJSS/V9I2/IAJSS0919